Quasiresonant laser-produced plasma: An efficient mechanism for localized breakdown

A. C. Tam
IBM Research Laboratory, San Jose, California 95193

(Received 19 February 1980; accepted for publication 27 May 1980)

This paper deals semiquantitatively with the phenomenon of quasiresonant laser-produced plasma (QRLPP) generation, i.e., breakdown of an atomic vapor when a laser beam couples a resonant excited state with a high excited state. The origin of the breakdown, threshold conditions for the breakdown, and the the effect of inducible absorption are discussed. Furthermore, the QRLPP may exhibit an unusual asymmetrical behavior (observed for a Cs plasma) when the single mode cw dye laser is tuned near the quasiresonant absorption line: on the low-frequency wing, "noise-reduction" effect for the transmitted beam is observed, while on the high-frequency wing, "self-oscillation" of the plasma is observed. The self-oscillation seems to result from a periodic plasma diffusion from the laser focus. The QRLPP, produced by cw or pulsed lasers, is a very efficient plasma generation mechanism which appears to be useful for many atomic vapors, and the potential applications are discussed.

PACS numbers: 52.50.Jm, 42.60.He

I. INTRODUCTION

Laser-induced gas breakdown has been extensively studied ever since high-intensity pulsed lasers have been developed. In applied science, the laser-plasma mechanism is important in various studies like laser fusion,[1] energy conversion,[2,3] optical switching,[4] and others; while in pure science, laser breakdown is involved in studies like ion spectroscopy[5] or afterglow kinetics.[6] Most of the earlier laser-plasma productions[7-10] utilized multiphoton excitation and inverse bremsstrahlung to couple the light energy into the electron kinetic energy. Measures,[11] and Yamada and Okuda[12] first recognized that resonant optical excitation of a vapor system [Fig. 1(a)] is a highly efficient method of producing ionization in the vapor; Lucatorto and McIlrath[13] first demonstrated the efficient resonant laser-produced plasma (RLPP) mechanism by totally ionizing a Na vapor by a pulsed dye laser tuned to the resonant Na transition at 5896 Å. Since then, further experimental evidence[14] of efficient resonant laser-plasma generation and extensive computer modeling[15,16] of this mechanism has been reported.

The phenomenon of RLPP has been observed[5,13] only for atomic systems of densities exceeding 10^{16} cm^{-3}. In these dense vapor systems, rapid collisions of the resonant excited atoms (produced from the ground state by the laser beam) with electrons provide an efficient means of conversion of the laser energy into the plasma energy. However, in a dense vapor system, another less well-known method for efficient laser-plasma generation is possible, which I shall call the quasiresonant laser-produced plasma (QRLPP) mechanism. In this method [Fig. 1(b)], the dense vapor is irradiated by a quasiresonant laser beam, which couples a resonant excited state (i.e., a state with strong dipole transition moment with the ground state) and a higher excited state. At low enough incident laser intensity I and low enough atomic density N, the laser should be nearly unabsorbed by the vapor, since the thermal population of the resonant excited state is very small (the energy interval between the resonant excited state and the ground state is much larger than the thermal energy). In QRLPP, a quasiresonant laser beam of sufficiently high I can turn (as explained below) the normally transparent vapor opaque and produce a plasma. Tam and Happer[17] first demonstrated that this is possible in an alkali metal vapor even for a weak cw laser beam (of power ~ 0.1 W) being used, if it is focused. The plasma is localized near the laser focus. This clearly shows the high efficiency of the QRLPP mechanism, because even low-power cw laser beams can be used.

Although both the QRLPP method and the RLPP method are very efficient mechanisms to convert photon energy into plasma energy, there is an important difference between the two methods: The quasiresonant laser is not absorbed except where the plasma is located; so an isolated

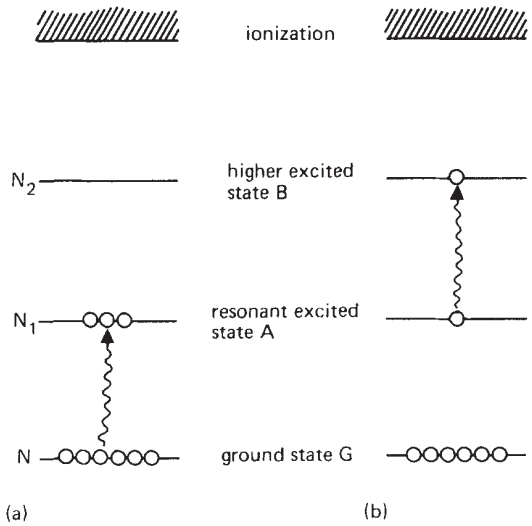

FIG. 1. Schematic of efficient laser production of plasma (a) by resonant excitation (RLPP), and (b) by quasiresonant excitation (QRLPP).

and highly localized plasma spark near the laser focus can be produced. On the other hand, the resonant laser is strongly absorbed by the unionized vapor, so that the plasma always extends from the incident window towards the interior of the vapor cell. Hence, when a localized "point source" of intense ionization is desired, the quasiresonant case is preferred. Such localized sources may find important applications in ion spectroscopy, energy conversion studies, plasma wave studies, or for providing ion beams for ion-beam microscopy, ion-beam lithography, or surface etching.

The QRLPP mechanism should be an important general method to produce localized plasmas in various atomic systems, and further experimental and theoretical understanding of the mechanism is desirable. I have[18] reported on the dynamic response of a QRLPP due to modulations of the laser beam, and the experimental observation[18] of a reduction in the laser beam modulation after transmission through the plasma provides semiquantitative support for a rate equation analysis to explain the plasma formation. Details of this analysis and of the QRLPP generation observed in a Cs vapor are reported in this paper.

II. THRESHOLD CONDITIONS

The QRLPP mechanism for an atomic vapor can be explained in the block diagram shown in Fig. 2. The laser is *not* absorbed by the ground-state atoms. However, through molecular aborption or collision-induced absorptions, a few atoms in the resonant excited state are produced by the laser light. These resonant excited atoms *do* strongly absorb the laser. At sufficiently large I and large N, a self-propagating cyclic reaction, initiated from the atoms in the resonant excited state can be produced, and this can cause most of the laser energy to be deposited in the medium and produce ionization. Threshold conditions in N and I must be satisfied for the cycle in Fig. 2 to become runaway.

Collisions for the production and heating of electrons are crucial for the generation and the maintenance of the QRLPP. The threshold conditions for the plasma production can be semiquantitatively understood as follows. At low atomic density N, the optically excited atom B decays mainly by radiative decay, with a lifetime τ_2^{rad}. If N is gradually increased, collisional excitation transfer becomes more and more important; in particular, associative ionization,[19,20]

$$X(B)+X(G)\rightarrow X_2^{+}+e, \tag{1}$$

becomes an important mechanism to produce electrons. Here, $X(B)$ and $X(G)$ are atoms of the element X in the B and G states, respectively. Equation (1) is energetically possible only if the B state is high enough in energy, i.e.,

$$\text{Ionization Energy of } B \text{ State} < \text{Binding Energy of } X_2^{+}. \tag{2}$$

For example, for the cases of the alkali atoms, binding energy of the molecular ion is ~ 1 eV.

In addition, to effectively produce ionization, the associative ionization collision rate must be sufficiently fast, i.e.,

$$N\alpha_{ai}\tau_2^{\text{rad}} \gtrsim 1, \tag{3}$$

where α_{ai} is the associative ionization coefficient for the B state and τ_2^{rad} is the radiative decay rate of the B state. As an example, in the Cs case with state B being the $8D_{3/2}$ excited state, $\alpha_{ai}\sim 10^{-10}$ cm^3 sec^{-1}, [19] and $\tau_2^{\text{rad}}\sim 10^{-7}$ sec; hence Eq. (3) corresponds to a threshold condition of

$$N \gtrsim 10^{17}\ \text{cm}^{-3}, \tag{4}$$

which is close to the typical threshold density for plasma production observed.[17]

The kinetic energy of the electron produced in Eq. (1) is typically much smaller than 1 eV, since it is equal to the difference of the binding energy of the molecular ion and the ionization energy of the B state. In order to cause efficient plasma production, an electron-heating mechanism is needed. This is possible when the laser intensity is high enough such that superelastic collisions of an electron with an $X(B)$ atom becomes highly probable, i.e.,

$$N_2 V_e \sigma_{e2} \tau_e \gtrsim 1, \tag{5}$$

where N_2 is the density of excited B state atoms, V_e, is the electron velocity, σ_{e2} is the average superelastic collision cross section of an electron with the B state, and τ_e is the electron lifetime (recombination or diffusion limited). The threshold condition (5) states that a sufficiently high laser intensity I is needed to produce sufficiently large N_2 to produce the plasma; however, Eq. (5) is not very useful as it is, since it involves the density N_2 (before plasma formation), which depends on the detailed production and destruction channels for the excited states before the plasma is produced. However, if the dependence of N_2 on I and N is known, then Eq. (5) provides an estimate of the threshold laser intensity I. For example, for the case of a Cs vapor excited by the 6010 Å laser,[17] we have

$$N_2 \approx N_1 \tag{6}$$

(i.e., the excitation $A \rightarrow B$ is saturated by the laser) under our typical experimental conditions. Now, before the plasma is formed, atoms in the A state are produced by the laser excitation of Cs_2 dimers. An order of magnitude estimate shows that the production rate of A atoms is $\sim 10^{-18}\ IN^2$, where I is the laser intensity in W cm^{-2}, and N is the ground-state atomic density in cm^{-3} (the Cs_2 density varies as N^2 approximately). We may assume that the decay rate of the A

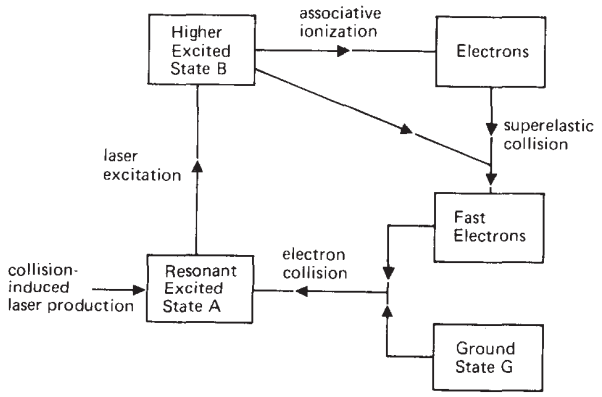

FIG. 2. Positive feedback cycle causing breakdown by quasiresonant laser excitation at sufficiently high atomic density and laser power.

state is the radiative decay rate (modified by radiation trapping) of $\sim 10^7$ sec^{-1}. Equating the production and decay rates for the A state, we have

$$N_1 \sim 10^{-25} I N^2. \tag{7}$$

Combining Eqs. (5)–(7), and assuming $V_e \sim 10^7$ cm sec^{-1}, $\sigma_{e2} \sim 10^{-14}$ cm^2 and $\tau_e \sim 10^{-6}$ sec (ambipolar-diffusion limited), we have the threshold condition being

$$10^{-38} I N^2 \gtrsim 1 \tag{8}$$

or

$$I \gtrsim 10^4 \ W \text{ cm}^{-2}, \tag{9}$$

if we put $N \sim 10^{17}$ cm^{-3}. This is close to the experimentally observed laser threshold, being ~ 0.1 W intensity focused to an area $\sim 10^{-5}$ cm^2. Note that the threshold laser intensity in Eq. (9) is some ten orders of magnitude lower than the conventional laser breakdown threshold due to multiphoton ionization and inverse bremsstrahlung.

Although Eqs. (4) and (9) are specifically for the Cs vapor, these values for the threshold density and laser intensity are expected to be typical for other vapors (alkali, alkali-earth, etc.), if the quasiresonant laser excitation is a strongly dipole-allowed line producing a sufficiently high excited state (whose ionization energy is less than the binding energy of the molecular ion).

III. KINETICS IN THE PLASMA; INDUCIBLE ATTENUATION

The previous section discusses the plasma threshold condition: at sufficiently high N and I, the optical excitation of an A atom will produce (through collisions involving electrons) an A atom again, and hence the cycle in Fig. 2 becomes runaway. After the laser plasma is produced, a large N_1 density is maintained by electron collisions, corresponding to the Boltzman distribution with an electron temperature T_e. Hence the laser is strongly attenuated by the plasma spark, and absorption is typically $\gtrsim 50\%$. It should be noted that the QRLPP is an inducible absorber, i.e., the percentage laser absorption quickly increases as laser power increases. This is in contrast to the more common case of bleachable absorption, when percentage absorption decreases with increasing laser power owing to saturation, optical pumping,

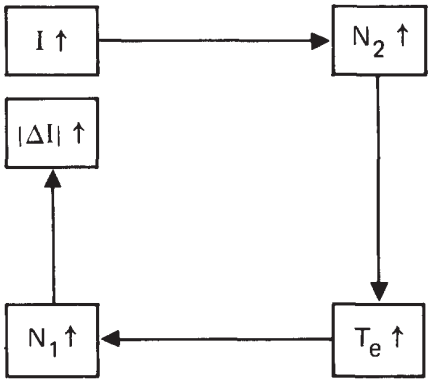

FIG. 3. Schematic to explain the inducible absorption behavior in quasiresonant laser-produced plasma.

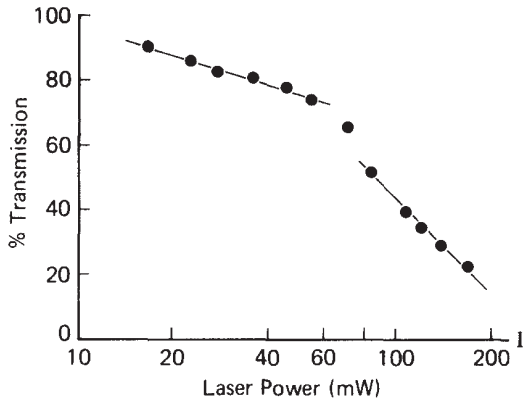

FIG. 4. Observed inducible absorption behavior in the QRLPP in a Cs vapor (at an atomic density of 10^{17} cm^{-3}) excited by a cw laser beam at 6010 Å ($8D_{3/2} \leftarrow 6P_{1/2}$ transition). A laser spark appears near the focus for laser power exceeding 70 mW.

or hole burning. The inducible absorption can be qualitatively explained by the reactions shown in Fig. 3. An increase in the laser intensity I produces a higher density N_2 through optical excitation; this causes a higher electron density through associative ionization and also a higher electron temperature by superelastic collisions; the resonant excited state density N_1 is thus increased by more frequent electron excitation from the ground state; this in turn causes an increase in the absorption $|\Delta I|$ due to an increase in N_1. Even a small increase in N_1 may cause a large change in $|\Delta I|$, which depends on N_1 exponentially. An example of the inducible absorption behavior observed for a Cs vapor is shown in Fig. 4: we see that the vapor is highly transparent to the quasiresonant laser beam in the low-intensity limit, but is opaque at sufficiently high intensity.

An interesting manifestation of the inducible-absorption behavior of a QRLPP is the automatic noise-reduction effect. The amplitude noise of the incident cw laser is greatly reduced on transmission through the plasma. To study this noise-reduction effect quantitatively, a sinusoidal modulation of a small fixed amplitude and variable frequency f is superimposed on the incident laser beam. The fractional modulation in the transmitted laser beam is found[18] to be much smaller than the fractional modulation in the incident beam for low f, but the two modulations are nearly equal at high f. The following simplified rate equation analysis of this noise-reduction effect and its dependence on f provides some insight into the QRLPP mechanisms.

Let the incident laser beam be weakly modulated,

$$I = I_0 + I' \exp(i\omega t), \tag{10}$$

where $\omega = 2\pi f$, I' is the amplitude of modulation which is much smaller than the steady component I_0, and it is understood that only the real parts of any complex quantities have physical meaning. The incident fractional modulation is m given by

$$m = I'/I_0. \tag{11}$$

The ac component I' of the incident light produces ac components N_2', N_e', and N_1' in the densities N_2, N_e, and N_1, which are densities of B atoms, electrons, and A atoms, re-

spectively. To simplify analysis, we assume that N_2 is characterized by a fast decay time τ_2 given by

$$1/\tau_2 = 1/\tau_2^{\text{rad}} + N\alpha_{ai} + 1/\tau_2^{\text{dif}}, \tag{12}$$

where terms on the right-hand side represent radiative decay rate, associative ionization rate, and diffusion rate out of the plasma volume. The rate equation for N_2 is,

$$dN_2/dt = BIN_1 - N_2/\tau_2, \tag{13}$$

where B is the Einstein absorption coefficient, and we have assumed that N_2 is small compared to N_1 because τ_2 is short. We further assume that the fractional modulation of N_1 is small compared to that in I, so that we may replace N_1 by N_{10}, the dc component. This assumption seems reasonable in the Cs case we have studied, since spatial diffusion and plasma volume expansion would limit the fractional increase in densities of excited species to be smaller than that in I. With those assumptions we may solve Eq. (13) and obtain

$$N_2 = N_{20} + N_2' \exp(i\omega t), \tag{14}$$

where

$$N_{20} = BI_0N_{10}\tau_2, \quad N_2' = BI'N_{10}\tau_2,$$

and ω is small enough so that $\omega\tau_2 \ll 1$.

The rate equation for N_e is approximately

$$dN_e/dt = N_2N\alpha_{ai} - N_e/\tau_e, \tag{15}$$

where τ_e is the decay time of the electron density, and is assumed to be diffusion limited (independent of the electron density). Substituting Eq. (14) into (15), we obtain

$$N_e = N_{e0} + \frac{N_e' \exp[i(\omega t - \phi)]}{[1 + (\omega\tau_e)^2]^{1/2}}, \tag{16}$$

where

$$N_{e0} = N_{20}N\alpha_{ai}\tau_e, \quad N_e' = N_2'N\alpha_{ai}\tau_e,$$

and

$$\phi = \tan^{-1}(\omega\tau_e). \tag{17}$$

ϕ is the phase delay of the electron density due to its comparatively slower decay rate (ambipolar diffusion rate of the electrons out of the laser focus volume of diameter $\sim 10^{-2}$ cm at a typical $N \sim 10^{17}$ cm^{-3} is $\lesssim 10^6$ sec^{-1}). Now, we further assume that the density N_1 is closely coupled to the electron density (because the resonant excited state is strongly produced from the ground state by electron collision), and that the decay rate of N_1 is faster than the decay rate of N_e. Thus, we have

$$N_1 = N_{10} + \frac{N_1' \exp[i(\omega t - \phi)]}{[1 + (\omega\tau_e)^2]^{1/2}}, \tag{18}$$

where N_{10} is the time averaged resonant excited density and N_1' is a coefficient for the modulated component of N_1 due to the modulation in the electron density.

The transmitted laser intensity I_t is,

$$I_t = I\exp(-N_1V), \tag{19}$$

where V is the product of the optical absorption coefficient and the path length. Substituting the real part of Eqs. (10) and (18) into Eq. (19), we have

$$\begin{aligned} I_t &= (I_0 + I'\cos\omega t)\exp\left[-N_{10}V - \frac{N_1'V\cos(\omega t - \phi)}{[1 + (\omega\tau_e)^2]^{1/2}}\right] \\ &\approx (I_0 + I'\cos\omega t)\left(1 - \frac{N_1'V\cos(\omega t - \phi)}{[1 + (\omega\tau_e)^2]^{1/2}}\right) \\ &\quad \times \exp(-N_{10}V) \\ &\approx \left[I_0 + I'\cos\omega t - \frac{N_1'I_0V\cos(\omega t - \phi)}{[1 + (\omega\tau_e)^2]^{1/2}}\right]\exp(-N_{10}V), \end{aligned} \tag{20}$$

where we have assumed that all modulated components are small and only first-order terms will be retained. We may rewrite Eq. (20) as

$$\begin{aligned} I_t \exp N_{10}V = I_0 + \Bigg[&\left(I' - \frac{I_0N_1'V}{1 + (\omega\tau_e)^2}\right)^2 \\ &+ \left(\frac{I_0N_1'V\omega\tau_e}{1 + (\omega\tau_e)^2}\right)^2\Bigg]^{1/2}\cos(\omega t + \psi), \end{aligned} \tag{21}$$

where

$$\tan\psi = \frac{I_0N_1'V\omega\tau_e}{[1 + (\omega\tau_e)^2]I' - I_0N_1'V}. \tag{22}$$

Equation (21) predicts that the transmitted fractional modulation is

$$m_t = \left[\left(m - \frac{\gamma}{1 + (\omega\tau_e)^2}\right)^2 + \left(\frac{\gamma\omega\tau_e}{1 + (\omega\tau_e)^2}\right)^2\right]^{1/2}, \tag{23}$$

where $m = I'/I_0$ is the incident fractional modulation, and

$$\gamma = N_1'V. \tag{24}$$

Equation (23) predicts that $m_t \to m - \gamma$ as $\omega \to 0$ and $m_t \to m$ as $\omega \to \infty$, which means that the transmitted fractional modulation is smaller than the incident fractional modulation at low modulation frequency, but the two fractional modulations become equal at high frequency. This behavior has been observed,[18] and the general dependence predicted by Eq. (23) (with γ and τ_e treated as parameters to fit the experimental data) has also been verified.[18] This good experimental fit is somewhat surprising in view of the several drastic assumptions made here to facilitate an analytical solution. A more detailed treatment, using numerical solutions of a more complete set of rate equations similar to the techniques of Measure *et al.*,[15] would be needed for a better understanding of the QRLPP mechanics. However, the present analytical treatment provides insight and qualitative understanding of the QRLPP mechanism.

IV. SELF-OSCILLATIONS OF cw PLASMA

Using a single mode cw dye laser turned near the 6010 Å quasiresonant absorption line of Cs, we have studied the dependence of the laser-plasma generation on the laser tuning. No external modulation is now applied to the incident laser beam. The transmitted laser intensity through the Cs vapor is shown in Fig. 5. When the laser is tuned on the low-frequency wing of the $8D_{3/2} \leftarrow 6P_{1/2}$ absorption line, the QRLPP is quiescent, and the transmitted laser exhibits the noise-reduction effect discussed in the previous section. However, when the laser is tuned to the high-frequency

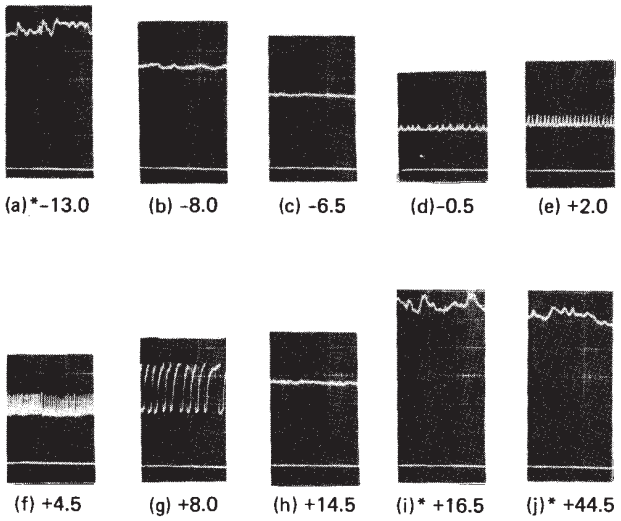

FIG. 5. Time variation of the transmitted laser beam (of power fixed at 170 mW) through the Cs vapor at 380 °C. The numbers indicated in (a) to (j) are detuning of the laser (in GHz) from the center of the absorption line. No plasma is formed in (a), (i), and (j) (denoted by asterisk). On the low-frequency wing [i.e., (b) and (c)] QRLPP is formed and noise reduction is observed in the transmitted beam. Near line center and on the high-frequency wing, (d)–(g), self-oscillation of the QRLPP occurs. For large positive detuning (h), no self-oscillation in the QRLPP is observed, but the plasma is "metastable", i.e., it is destroyed when the cw laser is momentarily interrupted. The horizontal time scale is 10 msec/cm, and the vertical scale (proportional to laser intensity) is constant in each scope picture, with the zero line given near the bottom.

wing, the transmitted laser beam shows regular modulation, indicating self-oscillations of the plasma.

In order to study the origin of the self-oscillation for high-frequency-wing excitation, spatially resolved fluorescence from the plasma is studied. The time-dependent fluorescence intensity F at 6973 Å is measured. F is proportional to the Cs*($7D$) excited state density, which is a measure of the electron temperature for a plasma in collisional equilibrium. We use a monochromator and photomultiplier to measure F from a small spot (of 0.1 mm size) at the laser focus. As shown in Fig. 6, F suddenly increases at the time of peak of the transmitted laser intensity, and then F decays back to its original value. This observation can be explained as follows: at a peak transmission of the laser, the intensity at the focus is maximum, since absorption upstream is smaller than average (to give peak transmission) and we assume negligible absorption downstream from the laser focus. Thus the plasma density at the focus suddenly increases, and subsequently the excess plasma density decays by diffusion. The slowing down of the diffusion rate as the Cs density N increases is clearly shown in Fig. 6: the decrease in fluorescence F (after the peak) has a time constant which is found to be proportional to N, indicative of a diffusion-controlled decay.

To show that plasma diffusion upstream is significant in the self-oscillating plasma, the fluorescence at different positions upstream from the laser focus is measured, as shown in Fig. 7. The onset of the increase in F and its subsequent decay is more and more time delayed (with respect to the transmission peak) as the observation point is further away from the laser focus. Indeed, the delay time τ between the transmis-

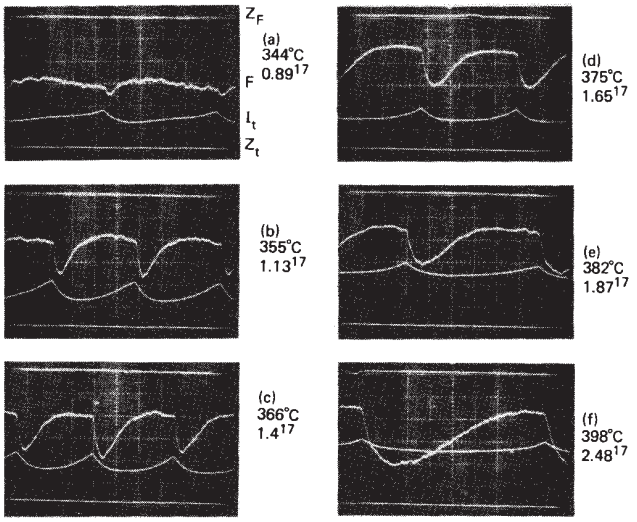

FIG. 6. Transmitted laser intensity (lower curve, marked I_t) and fluorescence at the laser focus (upper curve, marked F) in a QRLPP in Cs at various temperatures and atomic densities as given. The zero line for I_t is marked Z_t at the bottom, and the zero line for F is marked Z_F at the top (hence I_t and F increases in opposite directions). The horizontal time scale is 0.2 msec/cm for all the scope pictures shown, and the laser detuning is +4.5 GHz [i.e., case (f) in Fig. 5]. We clearly see that the decay time constant for the fluorescence increases linearly as N increases.

sion peak and the fluorescence peak varies as the square of the distance d upstream from the laser focus, and we find that

$$d^2/6\tau \approx D \approx 100 \text{ cm}^2/\text{sec}. \tag{25}$$

This again indicates that a random-walk-type diffusion up-

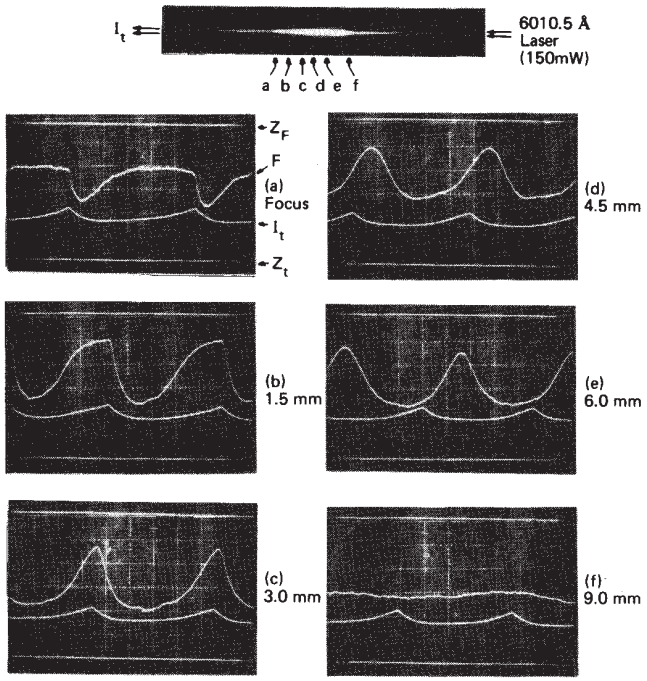

FIG. 7. Transmitted laser intensity (I_t) and fluorescence intensity (F) at various positions in the QRLPP. (a) gives F at the laser focus, while (b)–(f) give F at increasing distance upstream from the laser focus (the distance is indicated). The Cs density is fixed at 1.8×10^{17} cm^{-3}.

DOCKET ALARM

Explore Litigation Insights

Docket Alarm provides insights to develop a more informed litigation strategy and the peace of mind of knowing you're on top of things.

Real-Time Litigation Alerts

Keep your litigation team up-to-date with **real-time alerts** and advanced team management tools built for the enterprise, all while greatly reducing PACER spend.

Our comprehensive service means we can handle Federal, State, and Administrative courts across the country.

Advanced Docket Research

With over 230 million records, Docket Alarm's cloud-native docket research platform finds what other services can't. Coverage includes Federal, State, plus PTAB, TTAB, ITC and NLRB decisions, all in one place.

Identify arguments that have been successful in the past with full text, pinpoint searching. Link to case law cited within any court document via Fastcase.

Analytics At Your Fingertips

Learn what happened the last time a particular judge, opposing counsel or company faced cases similar to yours.

Advanced out-of-the-box PTAB and TTAB analytics are always at your fingertips.

API

Docket Alarm offers a powerful API (application programming interface) to developers that want to integrate case filings into their apps.

LAW FIRMS
Build custom dashboards for your attorneys and clients with live data direct from the court.

Automate many repetitive legal tasks like conflict checks, document management, and marketing.

FINANCIAL INSTITUTIONS
Litigation and bankruptcy checks for companies and debtors.

E-DISCOVERY AND LEGAL VENDORS
Sync your system to PACER to automate legal marketing.